# Effect of Polyvinylpyrrolidone Concentration in the Substrate of Thin-Film Composite Forward Osmosis Membrane on Neodymium Removal

**Yuan Xin Yeoh[1,2]\*, Mazrul Nizam bin Abu Seman[1,2]\*, Mohd Yusri bin Mohd Yunus[1,2] and Abdul Wahab Mohammad[3]**

[1]Faculty of Chemical and Process Engineering Technology, Universiti Malaysia Pahang Al-Sultan Abdullah, Lebuh Persiaran Tun Khalil Yaakob, 26300 Kuantan, Pahang, Malaysia
[2]Centre for Sustainability of Mineral and Resource Recovery Technology, Universiti Malaysia Pahang Al-Sultan Abdullah, Lebuh Persiaran Tun Khalil Yaakob, 26300 Kuantan, Pahang, Malaysia
[3]Chemical and Water Desalination Program, College of Engineering, University of Sharjah, Sharjah 27272, United Arab Emirates
\*Corresponding author (e-mail: nixyeoh@gmail.com; mazrul@umpsa.edu.my)

Secondary rare earth element (REE) resources need to be explored due to the increased global demand for REEs across all industries. Without the practice of a circular economy that fully utilises secondary REE resources, primary REE resources will deplete in the future. Therefore, this study suggests the recycling of REE from acid mine drainage (AMD) caused by mine tailings in upstream and midstream processes. This study implemented forward osmosis (FO) using a thin-film composite (TFC) membrane to remove neodymium (Nd) from synthetic AMD. The pore-forming agent, polyvinylpyrrolidone (PVP), with various concentrations, was used in the production of polyethersulfone (PES) porous substrate to serve as a support for the TFC FO membrane. A thin-film active layer of polyamide was formed on the top surface of the PES membrane support through the interfacial polymerisation method using 2 wt% of aqueous m-phenylenediamine and 0.15 wt% of trimesoyl chloride. The addition of PVP to the dope solution increased the substrate's porosity, making it more suitable for the FO process. The TFC FO PES membrane prepared from a substrate with 10 wt% PVP was proven to be the most effective in Nd removal, achieving 93.11% efficiency.

**Keywords**: Thin-film composite membrane; forward osmosis; membrane separation; rare earth element; neodymium separation

All non-renewable resources will deplete over time due to exploitation by human activities. Thus, most industries are trying to implement circular economy practices or explore other renewable resources. However, in the case of the rare earth element (REE) industry, there are no other replaceable materials for REEs due to their unique and irreplaceable physical and chemical characteristics. For instance, the most important application of REE is in clean energy technology, such as wind turbines and electric vehicles (EVs) [1].

As China is the largest producer of REEs globally, it was one of the first countries to focus on the circular economy. China utilised the most common technique in the circular economy, which involves retrieving REE from downstream processes. The REE recycling facilities collect and dismantle electronic waste (e-waste) to extract heavy metals and REEs using strong acids. A study was conducted in 2022 to evaluate the effect of REE downstream recycling in Guiyu town, which is the world's largest e-waste recycling base [2]. Surprisingly, the soil in Guiyu town was severely polluted by the recycling activities.

Therefore, a proper REE recycling method should be developed to preserve the reservoir of REE without causing any pollution to the Earth simultaneously. According to Gedam's team, the challenges faced by the mining industry in implementing circular economy include team management, economics, supply chain, social aspects, environmental concerns, technology and policy, financial issues, and infrastructure [3]. A research gap was identified in the team management and technology issues. Acid mine drainage (AMD) is a valuable secondary source of REE that is not utilised in conventional mining practices. Several studies have proven that AMD from different locations contains low concentrations of REEs [4, 5]. On the other hand, from the perspective of the mining industry, several problems are faced by the industry in closing the loop in the circular economy [3]. The first problem is poor team management, which lacks an AMD management plan as the generation of AMD is not planned before

371   Yuan Xin Yeoh, Mazrul Nizam bin Abu Seman,
      Mohd Yusri bin Mohd Yunus and
      Abdul Wahab Mohammad

Effect of Polyvinylpyrrolidone Concentration in
the Substrate of Thin-Film Composite Forward
Osmosis Membrane on Neodymium Removal

the mining process. The second problem is the industry does not consider the utilisation of mining waste beforehand due to a lack of appropriate technology. Thus, addressing the AMD issue can simultaneously resolve two challenges faced by the mining industry and further reduce pollution on Earth.

Rare earth element recovery from AMD and wastewater has been explored recently through adsorption [4, 6], ion exchange [5, 7], and membrane technology [8, 9]. Among all the technologies, membrane technology requires the least amount of chemicals as REE stripping is not needed. Membrane technology is well-known for being a clean, low-energy, and low-cost technology [10]. Among all widely available technologies for membrane separation, forward osmosis (FO) is the most suitable technology to concentrate REE in AMD with the objective of reducing pollution. This is because osmotic-driven FO does not require external pressure, unlike other external pressure-driven membrane technologies, such as reverse osmosis (RO) [11]. Salt is the most common solute used to create osmotic pressure in an FO process. Thus, FO requires less energy only for stirring and water movement, resulting in lower costs. At the same time, the absence of external pressure reduces the likelihood of membrane fouling. However, the effect of both internal concentration polarisation (ICP) and external concentration polarisation (ECP) is more severe in osmotic-driven membranes [12]. Although FO is typically utilised in seawater desalination [13, 14] and wastewater treatment [11], it can also be applied in concentration processes [15].

The current established work of REE concentration in AMD via FO is based on commercial membranes [9]. Thus, there is a lack of parameter studies on membrane support and active layers for REE concentration. It has been proven that the type of solvent, concentration of polymeric material, and type of additives are the main factors affecting the morphology of flat-sheet membrane support [16]. This study focused on the effects of polyvinylpyrrolidone (PVP) concentration in the membrane support of thin-film composite (TFC) FO membrane on neodymium (Nd) removal in synthetic AMD.

Previous studies have shown that the mixing of PVP in the dope solution can increase the void area in the membrane, enhance water permeability, and reduce the contact angle [17, 18]. Thus, PVP was proven to be a good pore-forming agent. The addition of PVP to the substrate of the TFC FO membrane can further increase water flux and permeability. Theoretically, a porous substrate has a lower structural parameter (S), which limits ICP [8] and provides higher water flux ($J_W$) [19]. Therefore, this work aims to study the effect of PVP concentration on Nd removal in synthetic AMD. Four different concentrations of PVP (0 wt%, 5 wt%, 10 wt%, and 15 wt%) were used to prepare polyethersulfone (PES) substrate in this work.

## EXPERIMENTAL

### Chemicals and Materials

Preparation of the dope solution for fabricating the membrane support layer involved the use of PES (Petronas BASF Malaysia) as the polymeric material, polyvinylpyrrolidone (PVP, MW 40 kDa, Sigma-Aldrich) as the pore-forming agent, and 1-methyl-2-pyrrolidinone (NMP, 99%, Sigma-Aldrich) as the solvent. The thin-film layer was prepared using m-phenylenediamine (MPD, flake, 99% Sigma-Aldrich), deionised (DI) water, 1,3,5-benzenetricarbonyl chloride (TMC, Sigma-Aldrich), and n-hexane (ACS reagent, Sigma-Aldrich). Preparation of the draw solution was done using ultrapure water and sodium chloride (NaCl, ACS reagent, Sigma-Aldrich). Preparation of synthetic AMD was carried out using neodymium (III) nitrate hexahydrate (99.9%, Sigma-Aldrich), sulphuric acid ($H_2SO_4$, 95–97%, Sigma-Aldrich), and DI water.

### Equipment

An IKA RW 20 digital overhead stirrer was used to stir the dope solution. A custom-made machine was utilised for membrane casting. A Memmert UFB 500 oven was used to dry the substrate and TFC. A Sterlitech CF042A cell assembly was utilised to place the membrane for Nd removal test and to perform a two-stage non-pressurised test. A Longer Pump BT100-1L peristaltic pump was used to provide flow into the cell assembly. An AND FX-3000i precision balance was utilised to detect the changes in weight of the draw solution before and after the Nd removal test and the two-stage non-pressurised test. An Eutech PC 2700 multi-parameter meter was used to measure the conductivity in the feed solution and the draw solution before and after the experiment. A Nicolet iS 5 Fourier transform infrared (FTIR) spectrometer was utilised to analyse the spectra of the substrate and TFC FO membrane. A Sterlitech HP4750 stirred cell was used for a dead-end filtration test. A ZEISS Merlin Compact field emission scanning electron microscope was used to study the membrane morphology. A Park NX10 atomic force microscope was used to study the surface roughness. A GENESYS 50 ultraviolet-visible (UV-Vis) spectrophotometer was utilised to determine the concentration of Nd in the feed solution and the draw solution before and after the experiment.

### Methodology

### Dope Solution Preparation

A dope solution was prepared from 17 wt% PES and different PVP concentrations (0 wt%, 5 wt%, 10 wt%, and 15 wt%) by mixing and stirring continuously

372　Yuan Xin Yeoh, Mazrul Nizam bin Abu Seman,
　　　Mohd Yusri bin Mohd Yunus and
　　　Abdul Wahab Mohammad

Effect of Polyvinylpyrrolidone Concentration in
the Substrate of Thin-Film Composite Forward
Osmosis Membrane on Neodymium Removal

with an overhead stirrer for 24 h at 40 °C. The homogeneous dope solution was degassed at room temperature for 6 h.

## Casting

The non-solvent-induced phase separation (NIPS) method was used to fabricate the flat-sheet substrate. The dope solution was poured onto a glass plate and cast into a membrane gel film using a semi-automatic casting machine with a gap size of 200 μm. Then, the cast film membrane was immersed in a non-solvent coagulation bath, which was DI water at room temperature, for a 15-min solidification process. Finally, the coagulation bath water was exchanged with new DI water, and the membrane was left for 24 h to ensure complete solvent exchange.

## Crosslinking of Polyamide Layer

For the preparation of a thin-film active layer on the top surface of the substrate via interfacial polymerisation (IP), excess water was removed from the surface using a rubber roller. Then, the substrate was fixed on an acrylic frame, and 50 mL of 2 wt% MPD aqueous solution was poured onto the top of the membrane support and left for 15 min. The excess MPD solution on the membrane surface was removed by tilting the frame vertically and using the rubber roller. Next, 30 mL 0.15 wt% of TMC in n-hexane was poured onto the top of the membrane support for the IP reaction for 60 s. The excess solution was removed by holding the membrane and frame vertically. Finally, the membrane was cured at 40 °C for 10 min and a polyamide (PA) thin-film active layer was formed on the top surface of the substrate.

## Characterisation Methods

### Membrane Porosity

The porosity ($\varepsilon$) of the substrate was determined through a simple wetting and drying test. The membrane was dried in an oven at 60 °C for a day to remove excess water in the pores. After weighing the dried substrate, it was immersed in DI water for a day. The wet substrate was weighed after wiping off the excess water from the surface using soft tissue. The porosity was calculated using Equation 1.

$$\varepsilon\,(\%) = \frac{w_w - w_d}{A_m \times l \times \rho_w} \times 100\% \qquad \text{Eq. 1}$$

## Mean Pore Size

A dead-end filtration cell was used to collect data on membrane flux, with DI water as the solution. One bar of nitrogen gas was applied to the filtration cell. The mean pore size ($r_m$) of the substrate was calculated using Equation 2.

$$r_m(m) = \sqrt{\frac{(2.9 - 1.75\varepsilon) \times 8\mu l Q}{\varepsilon \times A_m \times \Delta P}} \qquad \text{Eq. 2}$$

## Water Flux and Reverse Salt Flux

During FO and pressure-retarded osmosis (PRO), the mass of the draw solution was measured using a weight balance before and after the experiment to calculate the water flux using Equation 3.

$$J_W(L/m^2 \cdot h) = \frac{\Delta w}{A_m \cdot \Delta t \cdot \rho_w} \qquad \text{Eq. 3}$$

The reserve salt flux ($J_S$) can be determined from the experimental work using Equation 4. The salt concentration in the feed solution was determined by measuring the conductivity value and converting it to concentration using a standard calibration curve.

$$J_S(g/m^2 \cdot h) = \frac{C_{s,fs}(V_{0,fs} - J_w A_m t) - (C_{s0,fs}V_{0,fs})}{A_m \Delta t} \qquad \text{Eq. 4}$$

## Intrinsic Characterisation (A, B, S)

The feed and draw solutions were circulated in perpendicular flow within a membrane cell with a desirable orientation at a constant flow rate of 250 mL/min. For the intrinsic characterisation, ultrapure water was used as the feed solution, and NaCl with different concentrations (0.25 M, 0.50 M, 0.75 M, and 1.0 M) was used as the draw solution. The test was conducted in the PRO mode, where the active layer faces the draw side, to determine the values of water permeability (A) and solute permeability (B), followed by the FO mode, where the active layer faces the feed side to determine the value of S [20], as shown in Figure 1. The process was operated for 1 h after being stable for 5 min.
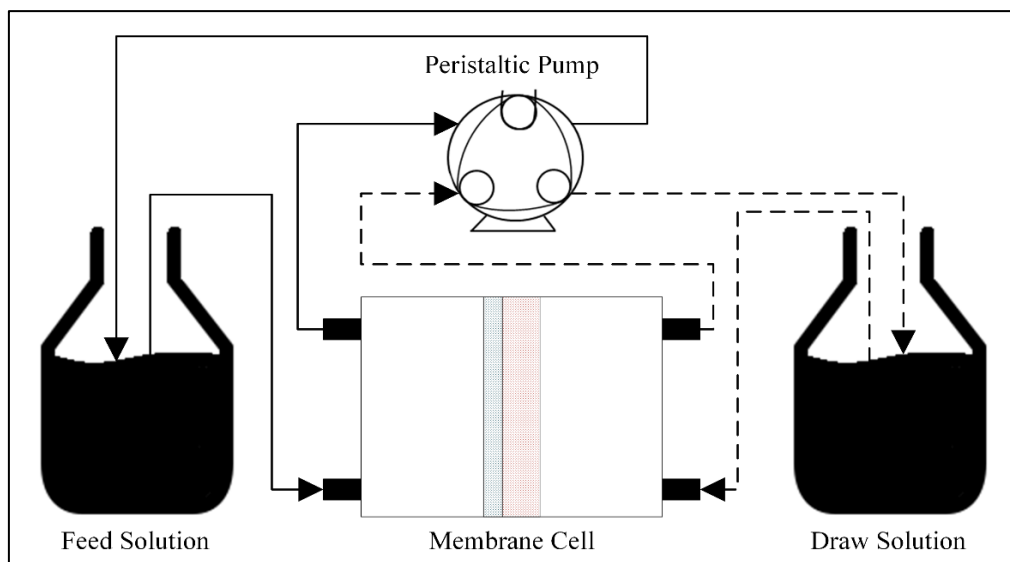
373 Yuan Xin Yeoh, Mazrul Nizam bin Abu Seman, Mohd Yusri bin Mohd Yunus and Abdul Wahab Mohammad

Effect of Polyvinylpyrrolidone Concentration in the Substrate of Thin-Film Composite Forward Osmosis Membrane on Neodymium Removal



**Figure 1.** Forward osmosis in AL-FS orientation

For the calculation of A, Equation 5 was applied when the effect of ECP is significant, which can be determined when the coefficient of determination ($R^2$) in corresponding linear graphs is higher than 0.9. When the effect of ECP is insignificant, Equation 6 was used instead.

For the calculation of B, Equation 7 was applied when the effect of ICP and ECP is significant, which can be determined when the $R^2$ in the linear line is higher than 0.9. When the effect of ICP and ECP is insignificant, Equation 8 was used instead.

The trial-and-error approach was used to calculate the value of S by applying Equation 9

using the experimental data obtained in the FO mode with different NaCl concentrations. Then, Equation 10 was applied with the ultimate aim of ensuring that the S value resulted in the minimum global error ($E_w$).

**Neodymium Removal**

For the Nd removal study, the FO mode was applied, as shown in Figure 1. The feed solution contained 100 ppm $Nd^{3+}$ at pH 5.0, while the draw solution contained 1 M NaCl. The concentrations of Nd in the feed solution before and after FO were determined using UV-Vis spectroscopy. Then, Equation 11 was used to calculate the removal efficiency [21].

$$J_w(L/m^2 \cdot h) = A\left[\pi_{D,b} \cdot exp\left(-\frac{J_w}{k}\right) - \pi_{F,b}\right] \qquad \text{Eq. 5}$$

$$J_w(L/m^2 \cdot h) = A \cdot \Delta\pi \qquad \text{Eq. 6}$$

$$B(L/m^2 \cdot h) = \frac{J_S}{C_{D,b} \cdot exp\left(-\frac{J_w}{k}\right) - C_{F,b} \cdot exp\left(\frac{J_w}{k}\right)} \qquad \text{Eq. 7}$$

$$J_S(g/m^2 \cdot h) = B \cdot \Delta C \qquad \text{Eq. 8}$$

$$J_w^C(L/m^2 \cdot h) = A\left[\frac{\pi_{D,b} \cdot exp\left(-\frac{J_w^E \cdot S}{D}\right) - \pi_{F,b} \cdot exp\left(\frac{J_w^E}{k}\right)}{1 + \frac{B}{J_w^E}\left[exp\left(\frac{J_w^E}{k}\right) - exp\left(-\frac{J_w^E \cdot S}{D}\right)\right]}\right] \qquad \text{Eq. 9}$$

$$E_w = \left(\frac{1}{n}\sum_{i=1}^{n}\sqrt{\left(1 - \frac{J_{w,i}^C}{J_{w,i}^E}\right)^2}\right) \times 100\% \qquad \text{Eq. 10}$$

$$Nd\ Removal\ Efficciency\ (\%) = \left(\frac{V_{f,fs} \times C_{Nd,f,fs}}{V_{0,fs} \times C_{Nd,0,fs}}\right) \times 100\% \qquad \text{Eq. 11}$$

374 Yuan Xin Yeoh, Mazrul Nizam bin Abu Seman,
Mohd Yusri bin Mohd Yunus and
Abdul Wahab Mohammad

Effect of Polyvinylpyrrolidone Concentration in
the Substrate of Thin-Film Composite Forward
Osmosis Membrane on Neodymium Removal

## RESULTS AND DISCUSSION

**Physicochemical Characterisation of Membrane**

The chemical structure of PES consists of three important functional groups, namely ether, phenyl, and sulfonyl groups, as depicted in Figure 2(a) According to a simplified correlation chart shown in Table 1 [22], the stretching of the C–O bond in ether can be observed between 1300 and 1000 $cm^{-1}$, the stretching of the C=C bond in phenyl at 1600 and 1175 $cm^{-1}$, and the stretching of the S=O bond in sulfonyl between 1350 and 1140 $cm^{-1}$. All of the aforementioned bonds can be observed at corresponding wavenumbers,

as shown in the FTIR spectra obtained in this study, which are depicted in Figure 3 in a straight line. Similar PES spectra were obtained in several studies [23-26].

Although PVP is soluble in water during the coagulation bath, the difference in FTIR spectra between the substrates suggests the presence of PVP. The only peak that was capable of distinguishing PVP from the PES spectra is 1662 $cm^{-1}$, as indicated by the dashed line in Figure 3. According to Table 1, the 1662 $cm^{-1}$ peak falls within the distinctive range of C=O stretching, confirming the presence of PVP, as C=O is not present in PES, as shown in Figure **2**.
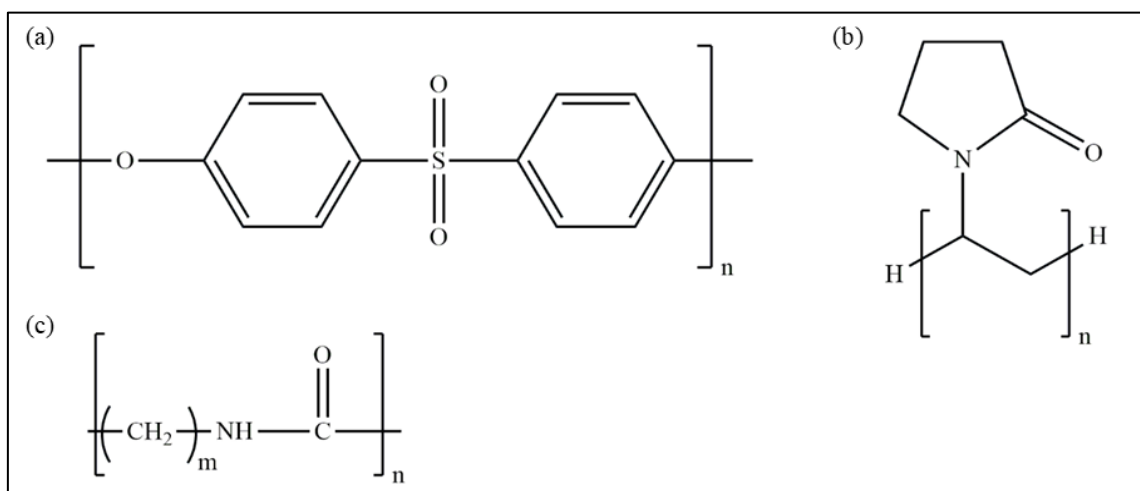


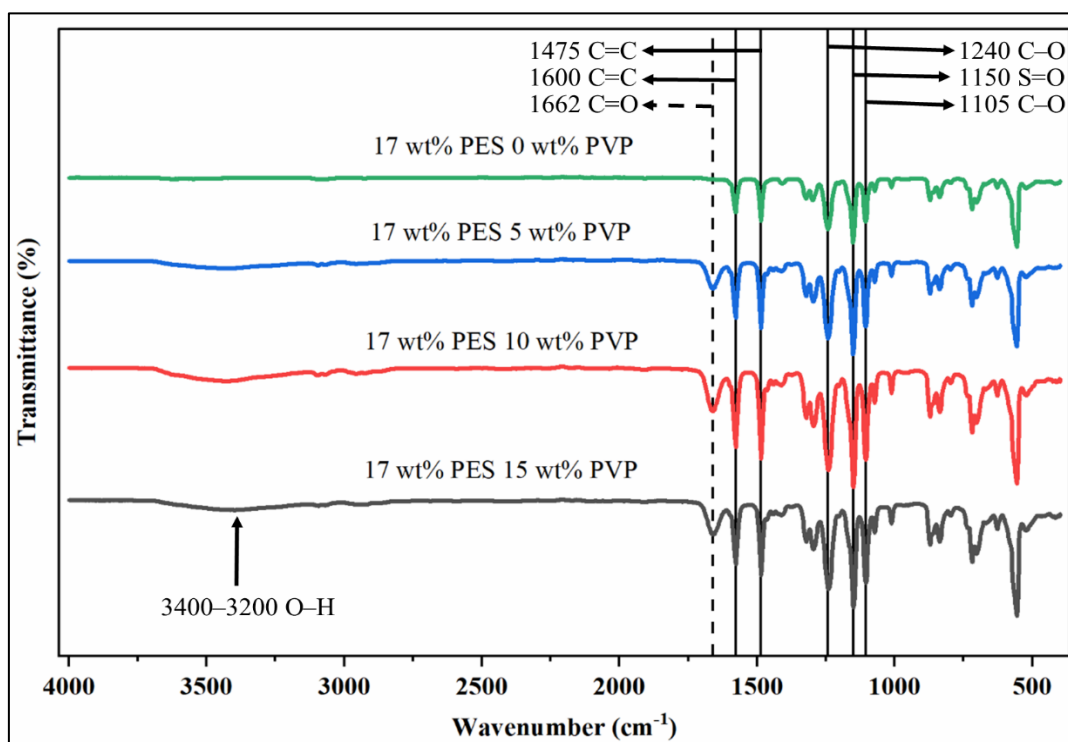**Figure 2.** Chemical structures of (a) PES, (b) PVP, and (c) PA.



**Figure 3.** FTIR spectra of PES membrane support with different PVP concentrations.

375   Yuan Xin Yeoh, Mazrul Nizam bin Abu Seman,                      Effect of Polyvinylpyrrolidone Concentration in
     Mohd Yusri bin Mohd Yunus and                                the Substrate of Thin-Film Composite Forward
     Abdul Wahab Mohammad                                         Osmosis Membrane on Neodymium Removal

**Table 1.** Infrared spectroscopy correlation [22].

| Wavenumber (cm$^{-1}$) | Bond | Type of Vibration | Functional Group |
|---|---|---|---|
| 3500–3100 | N–H | Stretching | Amide |
| 3400–3200 | O–H | Stretching | Amide |
| 1640–1550 | N–H | Bending | Amide |
| 1680–1630 | C=O | Stretching | Amide |
| 1600–1475 | C=C | Stretching | Phenyl |
| 1350–1140 | S=O | Stretching | Sulfonyl |
| 1300–1000 | C–O | Stretching | Ether |

The 1662 cm$^{-1}$ peak of PVP was also detected in other studies [25, 26]. In fact, there was another observable change in the spectra of the substrate containing PVP, which was observed at 3400–3200 cm$^{-1}$, representing the O–H stretching. However, neither PES nor PVP contains O–H stretching. The O–H stretching was contributed by the mesomeric structure of the hydrophilic PVP, which caused the C=O in pyrrolidone rings to temporarily bond with the water vapor in the air [27].

A thin layer of PA crosslinked on top of the substrate after IP. The comparison between the FTIR spectra of the PES substrate and the TFC membrane prepared from 15 wt% PVP is presented in Figure **4**. Unfortunately, as the C=O peak was the only one representing PVP, as discussed earlier, PVP could not be detected from the FTIR of the TFC membrane. This is because C=O also exists in PA, causing the peak to be indistinguishable. Similarly, the N–H stretching of PA should be observable between 3500 and 3100 cm$^{-1}$, but it overlapped with the aforementioned mesomeric structure of PVP in the same range. Therefore, the only obvious peak was the peak across the dotted line in Figure 4, located within 1640–1550 cm$^{-1}$, which represented the N–H bending [28, 29].
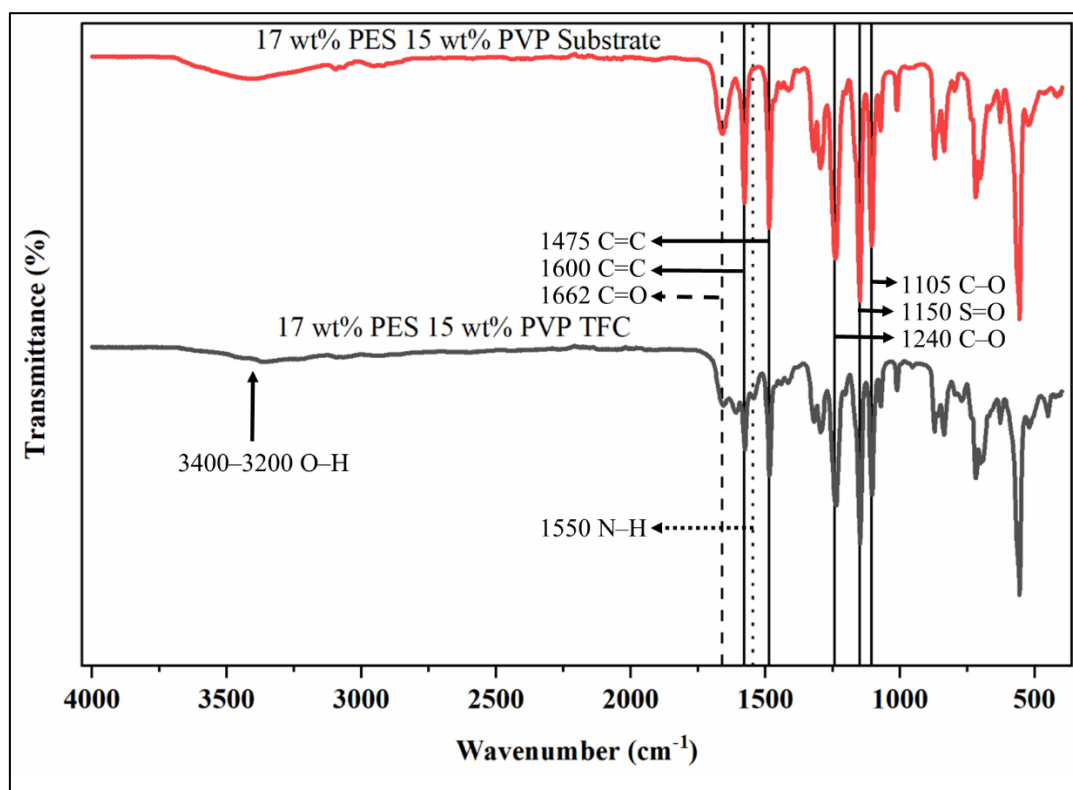


**Figure 4.** Comparison between FTIR spectra of PES substrate and TFC membrane prepared from 15 wt% PVP.
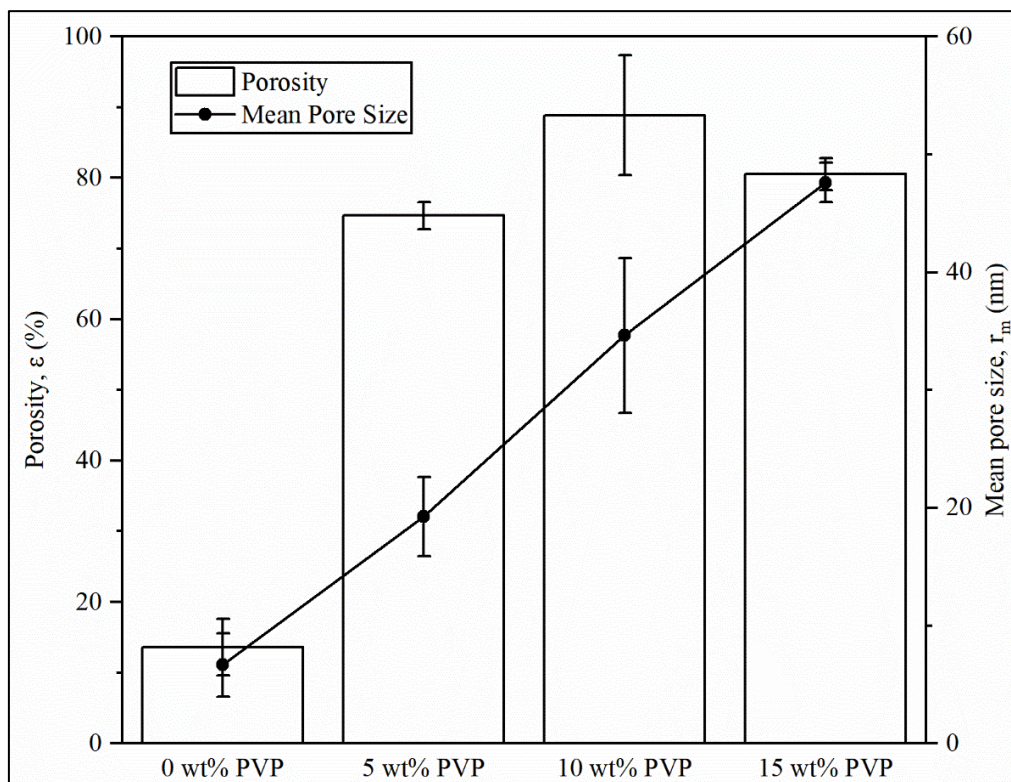
376  Yuan Xin Yeoh, Mazrul Nizam bin Abu Seman,
Mohd Yusri bin Mohd Yunus and
Abdul Wahab Mohammad

Effect of Polyvinylpyrrolidone Concentration in
the Substrate of Thin-Film Composite Forward
Osmosis Membrane on Neodymium Removal



**Figure 5.** Porosity and mean pore size of PES substrate with different PVP concentrations.

## Porosity and Mean Pore Size of the Substrate

With the addition of a pore-forming agent (i.e., PVP) in the dope solution, the porosity of the substrate increased drastically from 13.59% to above 74%, as shown in Figure 5. During solvent and non-solvent exchange, a significant amount of PVP, which is a water-soluble polymer, leached out from the semi-solidified dope solution, leading to the formation of pores [30]. However, some PVP remained in the substrate, as shown in Figure 3, which led to higher hydrophilic due to the nature of PVP. A decrease in porosity in the substrate was observed when 15 wt% of PVP was added to the dope solution. This phenomenon may be attributed to the high viscosity of the dope solution, which slowed down the demixing rate during phase separation [17, 31].

Referring to Figure 5, the mean pore size of the substrate increased linearly as the concentration of PVP increased. The increase in the mean pore size can be attributed to the high solubility of PVP in water. As the concentration of PVP increased, more void space was formed as PVP was leached out during phase separation, while the PES solidified slowly. Thus, a larger mean pore size was obtained as the concentration of PVP increased. All the substrates are suitable for IP as the pore size ranges between 1 and 100 nm [12].
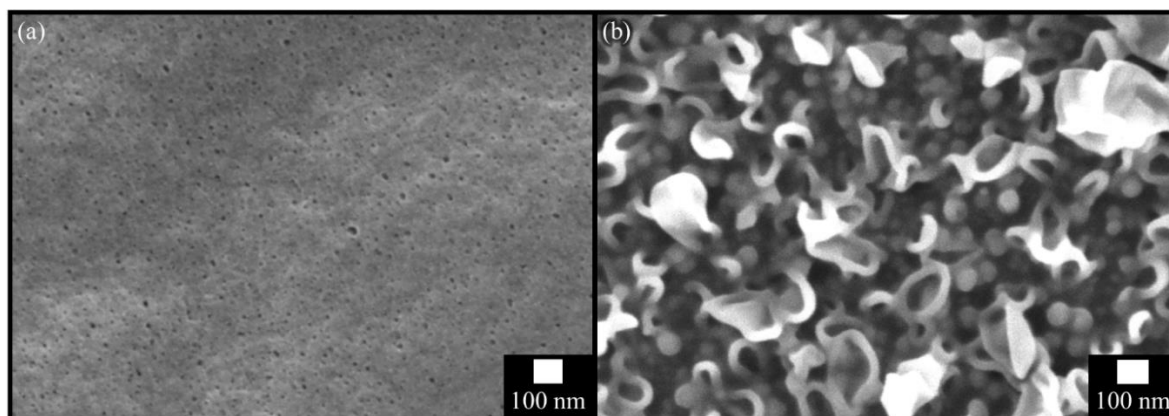


**Figure 6.** Field emission scanning electron microscopy (FESEM) images of the pristine PES membrane top surface at 50,000× magnification: (a) substrate and (b) TFC membrane.

377    Yuan Xin Yeoh, Mazrul Nizam bin Abu Seman,
       Mohd Yusri bin Mohd Yunus and
       Abdul Wahab Mohammad

Effect of Polyvinylpyrrolidone Concentration in
the Substrate of Thin-Film Composite Forward
Osmosis Membrane on Neodymium Removal

## Morphology of Membrane

The comparison between the top surface images of the substrate and TFC membrane is illustrated in Figure 6. The substrate surface is smooth and flat with some visible pores scattered, while the surface of the TFC membrane consists of typical leaf and nodule features, also known as a ridge-and-valley appearance. By right, the crosslinking of the PA layer should be flat and smooth on top of the substrate. However, the freshly formed PA thin-film layer was destroyed by the degassing of $CO_2$, $N_2$, and $O_2$ from the aqueous solution during IP, leading to the formation of a leaf-like structure [32]. The heat produced by IP caused a reduction in the solubility of the aforementioned gases in an aqueous solution. Moreover, the HCl produced during IP as a result of the hydrolysis of TMC also facilitated $CO_2$ degassing.

As proven by Figure 7, all the TFC membranes produced had an asymmetric structure. Without the addition of PVP, the substrate formed was very dense, as illustrated in Figure 7(a-ii), which explains the low porosity obtained in Figure 5. Additionally, a number of finger-like macrovoids can be observed from the top until the bottom of the membrane, and microvoids were formed beneath the top surface. The addition of PVP increased the size of the macrovoids towards the bottom as the rapid intrusion of non-solvent increased through the pores on the top surface [33]. However, the growth of macrovoids stopped when the PVP concentration increased to 15 wt%, as shown in Figure 7 (c-i). The high viscosity hindered the demixing rate and suppressed the formation of macrovoids, leading to the formation of a denser structure, as indicated by the decreased porosity shown in Figure 5. This is similar to another study that blended PVP in cellulose acetate (CA) [31]. The viscous dope solution also prevented the formation of microvoids beneath the top surface starting from 10 wt% of PVP due to the slow demixing [34]. The slow diffusional exchange rate between DI water and NMP also led to the formation of a spongy structure in the substrate with a thicker, denser skin at the top surface, as shown in Figure 7 (c-ii) and (d-ii). Thus, the porosity of the membrane increased significantly with the addition of PVP.
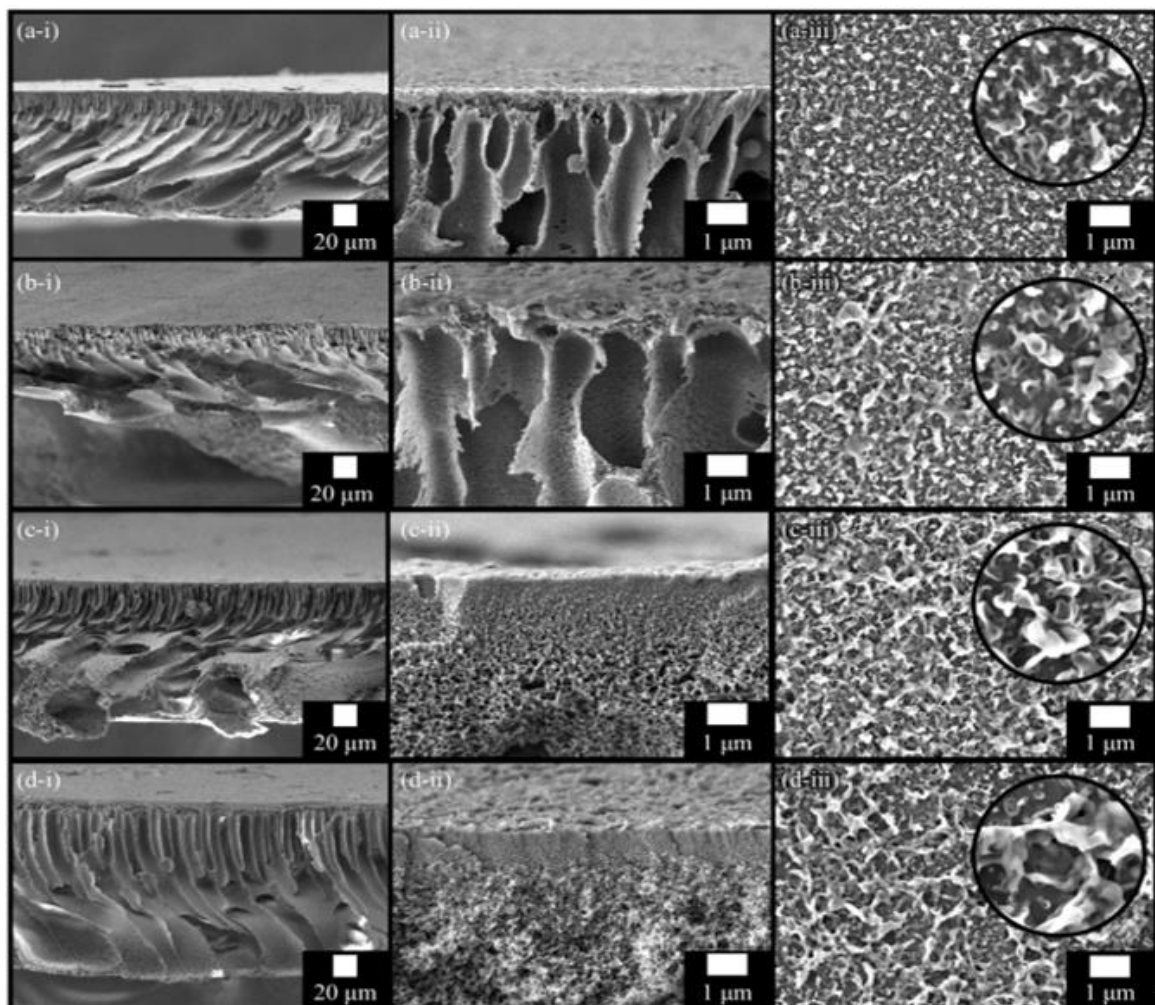


**Figure 7.** FESEM images of cross-sections with magnifications of: (i) 300× and (ii) 10,000× and top surface with magnifications of (iii) 10,000× and 50,000× (in circle) of PES TFC membranes produced from different concentrations of PVP: (a) 0 wt%, (b) 5 wt%, (c) 10 wt%, and (d) 15 wt%.

378    Yuan Xin Yeoh, Mazrul Nizam bin Abu Seman,                    Effect of Polyvinylpyrrolidone Concentration in
          Mohd Yusri bin Mohd Yunus and                              the Substrate of Thin-Film Composite Forward
          Abdul Wahab Mohammad                                       Osmosis Membrane on Neodymium Removal

For the effect of an increment in PVP concentration on the top surface, more voids (dark areas) can be observed as the nodules structure slowly grows from nodules to leaves, extended leaves, and finally, flat areas known as belts, as illustrated in Figure 7. A leaf-and-nodule-like structure can be observed in Figure 7(a-iii) with some extended leaves. However, more nodules and leaves grew into extended leaves, which further interconnected and developed into flat areas known as belts when the concentration of PVP increased, as depicted in Figure 7(b-iii) and Figure 7(c-iii). When 15 wt% PVP was used to prepare the membrane, nodules were hardly observed in Figure 7 (d-iii) as the belt structure developed and interconnected across the top surface. All the terms used to describe the shape of the PA layer formed were referenced from another study [35]. The change of the structure from nodules to belts with numerous visible voids can be attributed to the increase in mean pore size, which facilitated the diffusion of more MPD into the pores. Thus, more nanobubbles were released during IP, causing differences in the roughness features of each membrane [32, 36].

According to Figure 8, the ascending order of surface roughness (Ra) of the TFC membrane was as follows: 0 wt% (51.126 nm), 15 wt% (55.042 nm), 5 wt% (58.644 nm), and 10 wt% (77.707 nm). The Wencel relation suggests that roughness can enhance either hydrophilicity or hydrophobicity, depending on the nature of the surface [37]. As both PES and PVP are hydrophilic, a rougher surface improved the hydrophilicity of the membrane, leading to the high water flux obtained by the 10 wt% PVP TFC as it has the roughest surface. Moreover, surface roughness can also predict the membrane fouling tendency, as a rough membrane is more prone to fouling than a smooth membrane [19].

The structure obtained using atomic force microscopy (AFM) in Figure 8 does not seem to match the shape of the PA layer obtained in Figure 7 (iii). However, this discrepancy can be explained by the limitations of AFM [35]. The image captured using AFM depends on the contact between the pyramidal tip and the TFC membrane surface, facilitated by the oscillation of the cantilever. Therefore, the void, nodule, or leaf structures that were shielded by the extended leaf or belt structure are not visible in AFM. In fact, the hidden structures are supposed to be underneath the light lumps in AFM. The nodules and leaves of the TFC membrane prepared from 0 wt% PVP substrate in Figure 7 (a-iii) are well-presented in Figure 8 (a) as the number of extended leaves is limited. For the case of 5 wt% PVP, a ridge-and-valley structure was obtained, as shown in Figure 8 (b). This structure can be explained by the development of interconnecting belt structures in some areas, while the nodule and leaf structures were still visible in other areas in Figure 7 (b-iii).
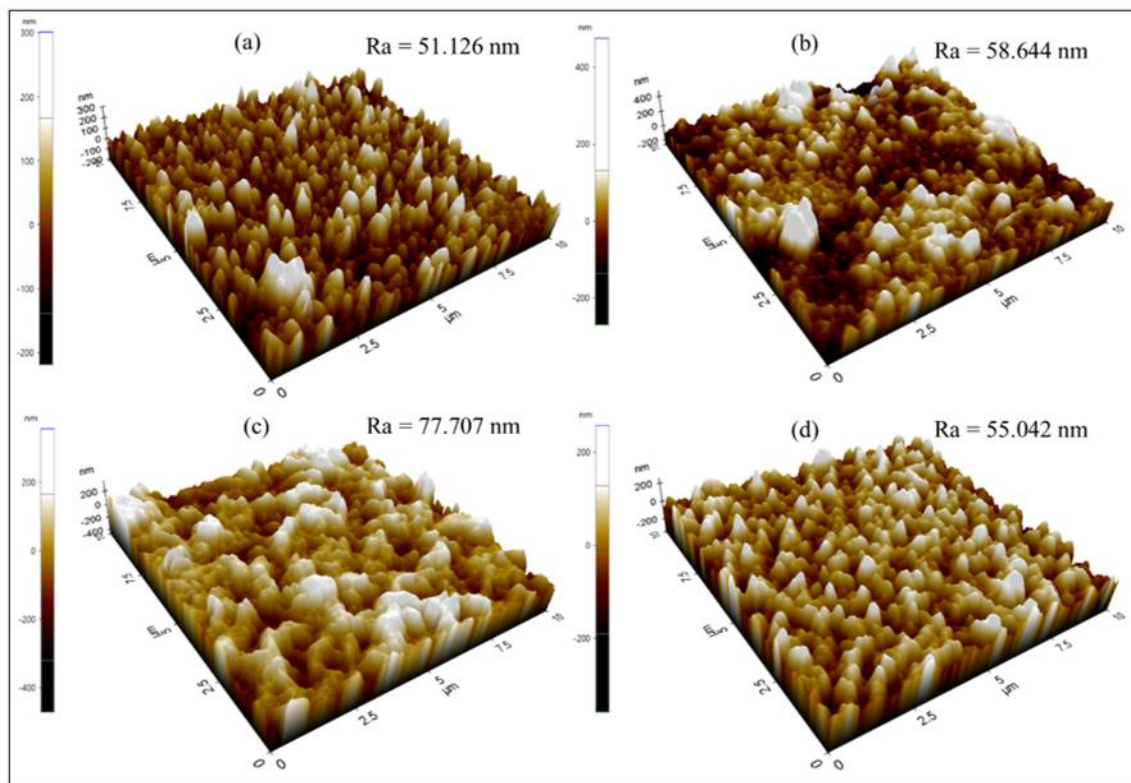


**Figure 8.** Three-dimensional AFM images of PES TFC membranes produced from different PVP concentrations: (a) 0 wt%, (b) 5 wt%, (c) 10 wt%, and (d) 15 wt%.

379    Yuan Xin Yeoh, Mazrul Nizam bin Abu Seman,
       Mohd Yusri bin Mohd Yunus and
       Abdul Wahab Mohammad

Effect of Polyvinylpyrrolidone Concentration in
the Substrate of Thin-Film Composite Forward
Osmosis Membrane on Neodymium Removal

Meanwhile, for 10 wt% PVP, all peaks were replaced by lumps, as shown in Figure 8 (c), as more belt structures were formed and connected in Figure 7 (c-iii). Lastly, the decrease in surface roughness for 15 wt% PVP suggested the rupture of the roughness structure, leading to a distinct spider-web-like structure as shown in Figure 7 (d-iii). However, this structure failed to be captured by AFM in Figure 8 (d) due to the aforementioned limitation, and a peak-like structure was captured instead because of the height difference of the PA layer belt structure.

**Water Flux and Reverse Salt Flux**

The water flux ($J_W$) of TFC FO membranes with substrates fabricated from different PVP concentrations is depicted in Figure 9. The result of the TFC FO membrane fabricated using 0 wt% PVP was not presented as there was no permeation across the membrane throughout the experimental work. This was due to the small mean pore size, low substrate porosity, and the dense PA thin-film active layer. The small mean pore size and porosity caused the confinement effect, hindering the degassing during IP and resulting in the formation of a thick and dense PA layer. Another study on ultrafiltration also failed to apply pristine PES substrate due to the dense skin layer [18]. The addition of PVP is necessary to fabricate a membrane substrate suitable for FO applications, which is an osmotic-driven process.

In both FO and PRO modes, the water flux increased as the concentration of NaCl in the draw solution increased in all membranes due to the increment of osmotic pressure [38, 39]. The osmotic pressure is closely related to the concentration of solute in a solution, as proven by the Van't Hoff equation [40]. A similar trend was observed by Ma's team that varied the concentration of NaCl from 0.5 M to 2.0 M, which resulted in an increase in water flux due to the higher osmotic pressure in both simulation and experimental studies [41].

The existence of ECP and ICP accounts for the reduction in effective osmotic pressure, resulting in lower water flux [42]. In the PRO mode, the impact of ICP is lower than in the FO mode [43] and has a higher effective osmotic pressure [19], which explains the higher water flux of PRO in all cases. Zhao's work showed similar results to this study, where the water flux in the FO mode was lower than in the PRO mode due to ICP. However, the water flux in PRO dropped faster than in FO, which indicated a severe fouling problem in the PRO mode [44]. Therefore, the FO mode is favoured over the PRO mode in separation processes involving high foulant despite lower water flux, as it can lead to a more stable water flux with lower fouling [45].

Also, a porous substrate is favourable for low ICP [19]. In both FO and PRO modes, the

TFC membrane prepared from the most porous substrate (10 wt% PVP) provided the highest water flux due to the low ICP, which allowed for high effective osmotic pressure, followed by the TFC membranes prepared from 15 wt% PVP and 5 wt% PVP. It can be interpreted that the higher the concentration of PVP, the more porous the membrane substrate becomes. This is because PVP acts as a pore-forming agent, directly increasing the pore size and porosity. However, when the PVP concentration is too high, the opposite effect occurs. A high concentration of PVP increases the viscosity of the dope solution, slowing down the demixing and precipitation rate during membrane fabrication [17]. This explains the reduction in water flux for the TFC membrane prepared with 15 wt% PVP. This can be supported by the simulation conducted by Lee's team to study the effect of surface porosity and bulk porosity [46]. From the study, an increase in both porosities led to a higher water flux. However, when the porosity was constant, the surface porosity led to an increase in water flux as the concentration of the draw solution increased, while the effect of manipulating bulk porosity was only noticeable at high concentrations of the draw solution and high surface porosity. Also, the ICP was lower in substrates with higher bulk porosity. In this work, bulk porosity was determined in Figure 5, showing the same trend as the water flux. In addition, the surface porosity can be estimated from Figure 7 (b), where the TFC membrane prepared with 10 wt% PVP has a more porous top surface than the one prepared with 15 wt% PVP, with the aim of enhancing its water flux. It is worth noting that the TFC prepared with 10 wt% PVP also has the roughest surface due to the belt and extended leaf structure, which improved its hydrophilicity [37].

However, there was one exception: the water flux of the substrate fabricated from 10 wt% PVP in the FO mode was lower than that of the substrate fabricated from 15 wt% PVP. This issue may be attributed to the low reverse salt flux in the substrate from 15 wt% PVP, as the top layer was sufficiently dense to prevent salt penetration. Another explanation could be that the effects of ECP and ICP for both membranes with 0.25 M NaCl as the draw solution were not significant.

For the case of reverse salt flux ($J_S$), two similar trends as water flux were observed: 1) Higher reverse salt flux was observed as the concentration of the draw solution increased, and 2) the reverse salt flux of the PRO mode was higher than that of the FO mode at the same draw solution concentration for the same membrane. The first trend could be explained by the increase in osmotic pressure, as the exact same trend was obtained in another study that used NaCl as the draw solution, but the concentration varied from 0.5 M to 2.0 M [41]. For the second trend, a higher reverse salt flux in the PRO mode was related to the low ICP compared to the FO mode. The same trend was observed in another study [47].
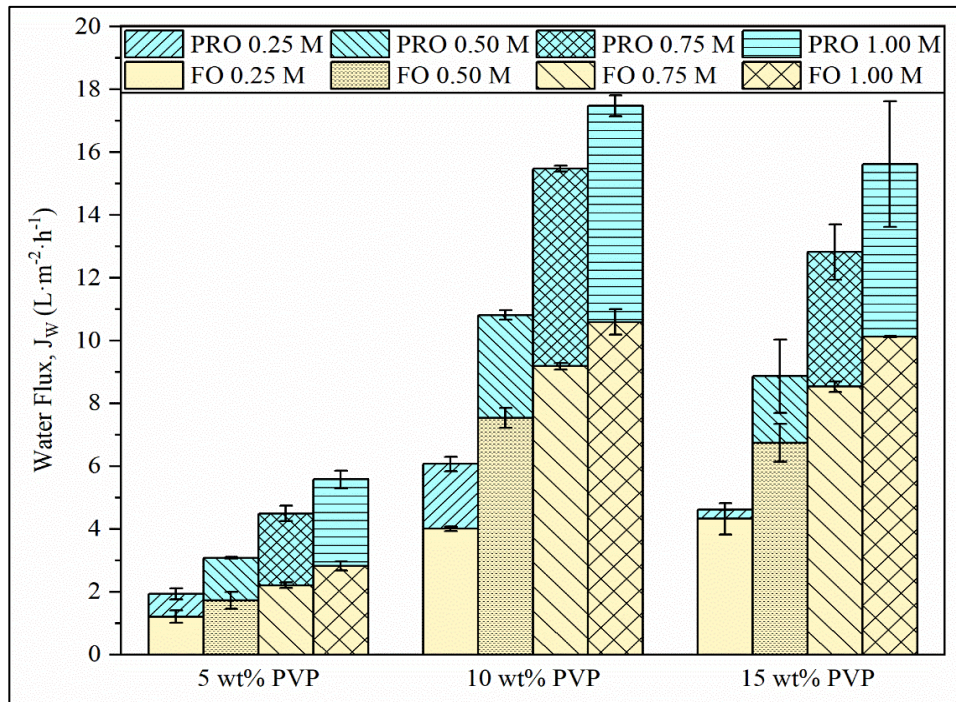
380   Yuan Xin Yeoh, Mazrul Nizam bin Abu Seman,
       Mohd Yusri bin Mohd Yunus and
       Abdul Wahab Mohammad

Effect of Polyvinylpyrrolidone Concentration in
the Substrate of Thin-Film Composite Forward
Osmosis Membrane on Neodymium Removal



**Figure 9.** Water flux of TFC FO membranes prepared from different PVP concentrations.

For the effect of PVP concentration, the substrate fabricated from 10 wt% PVP exhibited the highest reverse salt flux in both FO and PRO modes, as illustrated in Figure 10. The porous top layer of the 10 wt% PVP substrate could not prevent the permeation of salt when water diffused into the membrane draw solution in both FO and PRO modes. A study found a higher reverse salt flux in the TFC membrane prepared from substrates with higher porosity, which can be explained by the lower resistance for salt diffusion and an increase in convective salt diffusion due to a higher water flux [48]. On the other hand, different trends were observed for the membrane substrate fabricated from 5 wt% PVP and 15 wt% PVP when operated in both modes. The trend in the FO mode can be explained by the higher porosity of the substrate prepared from 10 wt% PVP. Meanwhile, the trend in the PRO mode can be explained by the morphology of the substrate. Theoretically, the TFC membrane prepared from the 5 wt% PVP substrate with a smaller mean pore size should exhibit superior performance in reverse salt flux due to the formation of a thicker PA layer [49]. However, in this study, an opposite trend was observed as the reverse salt flux of 15 wt% PVP was lower than that of the reverse salt flux of 5 wt% PVP, despite having a larger mean pore size. The phenomenon was influenced by the thick top layer of the 15 wt% PVP substrate, as illustrated in Figure 7 (d-ii), as compared to the thin top layer of the 5 wt% PVP substrate shown in Figure 7 (b-ii). The outlier of reverse salt flux in the 15 wt% TFC membrane for 0.25 M NaCl may be caused by the insignificant ICP and ECP at lower osmotic pressure.

Several factors may have contributed to the large standard deviation obtained in Figure 10. The first factor is the existing deviation in mean pore size and porosity, as illustrated in Figure 5. The deviation of the aforementioned parameters directly affected the substrate morphology. Judging from the small standard deviation of water flux in Figure 9, the deviation in reverse salt flux may originate from the structural differences in the substrate's top layer, as it failed to retain the diffusion of salt across the membrane. The second factor is that the membrane was hand-cast in this study. Most of the studies on TFC membranes either purchased commercial TFC membranes or performed IP on commercial substrates. Hand-cast membranes have different morphologies because various parameters can affect the morphology of the substrate. For instance, the angle of immersion, speed of immersion, volume of coagulation bath, coagulation bath temperature, time taken for the cast gel to be brought into contact with a non-solvent, air humidity, impurities on the surface of support used for casting, and others. All these parameters can be controlled more easily by using a machine to produce membranes with similar morphology. However, the use of commercial TFC membranes does not guarantee the reduction or elimination of standard deviation. A large standard deviation in a single point was obtained in a pilot-scale study using cellulose triacetate (CTA) membrane, even though a membrane from the same supplier was used [50]. The final factor is a limited sample size. The experimental work in this study was only repeated twice. The standard deviation may be reduced with more data collection.
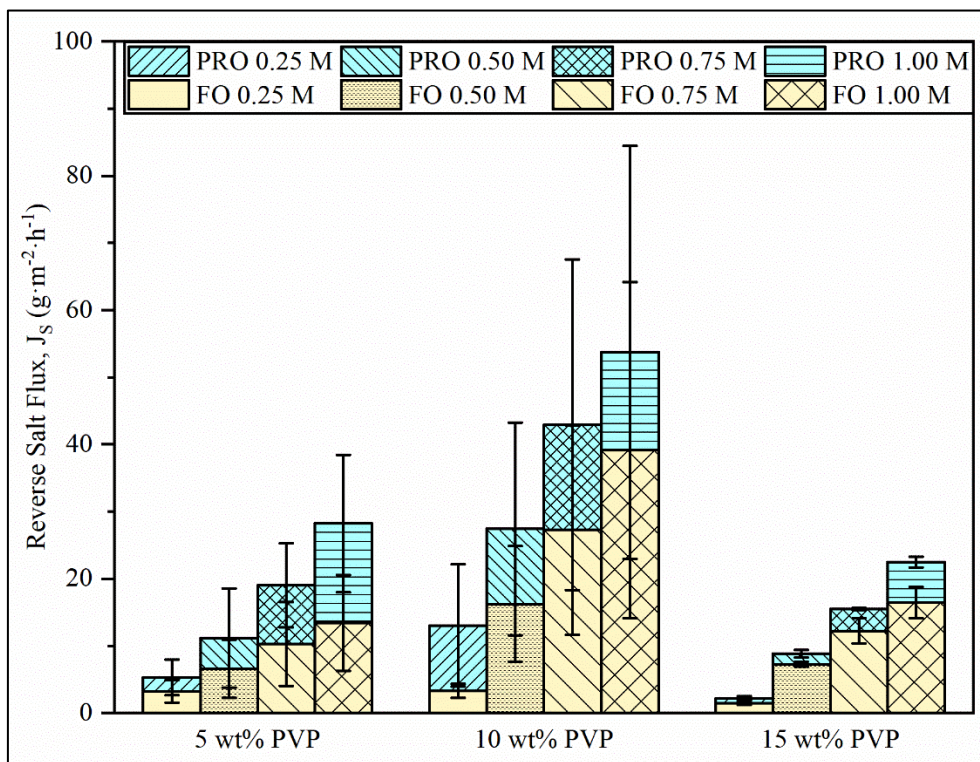
381   Yuan Xin Yeoh, Mazrul Nizam bin Abu Seman,
      Mohd Yusri bin Mohd Yunus and
      Abdul Wahab Mohammad

Effect of Polyvinylpyrrolidone Concentration in
the Substrate of Thin-Film Composite Forward
Osmosis Membrane on Neodymium Removal



**Figure 10.** Reverse salt flux of TFC FO membranes prepared from different PVP concentrations.

The ratio of reverse salt flux to water flux, known as specific reverse flux, can be used to assess the ability of the TFC membrane to prevent the penetration of NaCl across the membrane as water moves from the feed side to the draw side. As the FO mode was applied for Nd removal, the specific reverse flux was compared in the FO mode only, as shown in Table 2. As the concentration of PVP in the dope solution increased, the specific reverse flux decreased, indicating that less mass of salt in grams was transported from the draw side to the feed side for every litre of water transported from the feed side to the draw side. Increasing the concentration of NaCl will directly increase the osmotic pressure. Thus, the specific reverse flux increased simultaneously with the increment of NaCl. The TFC FO membrane prepared from a substrate with 15 wt% PVP exhibited the best specific reverse flux, indicating that the thick top layer, as depicted in Figure 9 (d-ii), has the ability to prevent the penetration of most salts in FO.

**Intrinsic Parameters of TFC Membrane**

There are three intrinsic parameters for the study of TFC membranes: water permeability (A), solute permeability (B), and structural parameter (S). A is also known as the hydraulic permeation coefficient of the active layer, while B is also known as the solute permeation coefficient of the active layer. S represents the mass transport resistance in an asymmetric membrane by measuring the actual distance of water permeation across the support membrane or the degree of ICP [51]. The most ideal intrinsic parameters are high A with low B and S.

**Table 2.** Specific reverse flux of TFC membranes prepared from different PVP concentrations at different NaCl concentrations in FO mode.

| Concentration of PVP in Dope Solution (wt%) | Specific Reverse Flux (g/L) at Different Concentrations of NaCl (M) | | | |
|---|---|---|---|---|
| | 0.25 M | 0.50 M | 0.75 M | 1.00 M |
| 5 | 1.8634 | 2.9929 | 3.6537 | 5.7092 |
| 10 | 0.8226 | 2.1535 | 2.9673 | 3.6951 |
| 15 | 0.3464 | 1.0778 | 1.4350 | 1.6250 |

382    Yuan Xin Yeoh, Mazrul Nizam bin Abu Seman, Mohd Yusri bin Mohd Yunus and Abdul Wahab Mohammad

Effect of Polyvinylpyrrolidone Concentration in the Substrate of Thin-Film Composite Forward Osmosis Membrane on Neodymium Removal

**Table 3.** Values of A, B, S, and $E_W$ of TFC membranes prepared from different PVP concentrations.

| Concentration of PVP in Dope Solution (wt%) | A (L/m²·h·bar) | B (L/m²·h) | S (μm) | $E_w$ (%) |
|---|---|---|---|---|
| 5 | 0.1368 | 0.5175 | 1715.2939 | 16.8296 |
| 10 | 0.6085 | 1.4826 | 467.5225 | 7.1416 |
| 15 | 0.4853 | 0.5105 | 445.7292 | 4.4247 |

As shown in Table 3, the TFC membrane prepared from 10 wt% PVP had the highest A, followed by substrates prepared from 15 wt% and 5 wt% PVP. This can be related to the water flux shown in Figure 11, which shows the same trend as both parameters are measures of water permeation across the TFC membrane. However, in the case of B, the TFC membrane with a substrate prepared from 10 wt% PVP had the highest B, followed by substrates prepared from 5 wt% and 15 wt% PVP. Similar to A, B is also closely related to reverse salt flux. By referring to Figure 10, the reverse salt flux of the TFC membrane prepared from 15 wt% PVP showed a slight difference compared to the TFC membrane prepared from 5 wt% PVP, which aligned with the B value.

For structural parameters, the trial-and-error approach was applied until the lowest global error ($E_W$) was achieved, as shown in Table 3. It can be interpreted that the effect of ICP was the highest in the TFC membrane prepared from a substrate with 5 wt% PVP, followed by 10 wt% and 15 wt% PVP. The structural parameters are inversely proportional to water flux and water permeability [19]. When S is low, the ICP is limited, allowing high water permeability and water flux, as demonstrated by the TFC membrane prepared from substrates with 10 wt% PVP and 15 wt% PVP. Based on the results of A, B, and S, the TFC membrane prepared from a substrate with 15 wt% PVP is the best membrane as it has a high A value and the lowest B and S values.

**Neodymium Removal**

Nd removal was carried out in the FO mode to benefit from lower reverse solute flux and fouling, using 1 M NaCl as the draw solution. The highest Nd removal of 93.11% was obtained when the TFC membrane was prepared from a substrate of 10 wt% PVP, followed by 5 wt% PVP (87.07%) and 15 wt% PVP (86.44%), as shown in Figure 11. The first possible explanation for the observed trend is the difference in the morphology of the PA thin-film active layer, as illustrated in Figure 7(iii). The belt and extended leaf structure of 10 wt% PVP may block the permeation of Nd ions across the membrane, while the ruptured structure of 15 wt% PVP, as well as the nodules and extended leaf structures, were not able to remove Nd. Jang's team mentioned that organic removal efficiency was related to the mean pore size [52]. However, the theory does not apply to this study as the Nd removal efficiency was almost similar for the TFC membrane with a thin dense PA layer prepared from 5 wt% and the TFC membrane with a thick porous PA layer prepared from 15 wt% PVP. Furthermore, 10 wt% PVP had an almost similar structure to 15 wt% PVP, as shown in Figure 7(ii). Therefore, another logical explanation related to Nd removal is the surface charge of the top surface. Based on the Nd removal efficiency obtained in this study, it can be estimated that the TFC membrane prepared from 10 wt% PVP has a low negative or positive surface charge, which repelled Nd ions. Conversely, the surface charge of the TFC membranes prepared from 5 wt% PVP and 15 wt% PVP could have a similar negative surface charge, attracting Nd ions and resulting in lower removal efficiency. The surface charge can be determined by measuring the zeta potential. However, there is no clear indication of the relationship between the morphology of an uncharged membrane and zeta potential. On the other hand, it is clear that the pH of a solution can directly affect the zeta potential of the membrane, with higher pH leads to a more negative zeta potential [53, 54]. The REE removal efficiency in another FO study showed that the concentrations were higher than 82% for all cases, with the removal of dysprosium (Dy) being the highest in the FO mode at 96% [9]. Therefore, pH can be used to modify the zeta potential of the membrane to enhance the removal efficiency of REEs in the future.
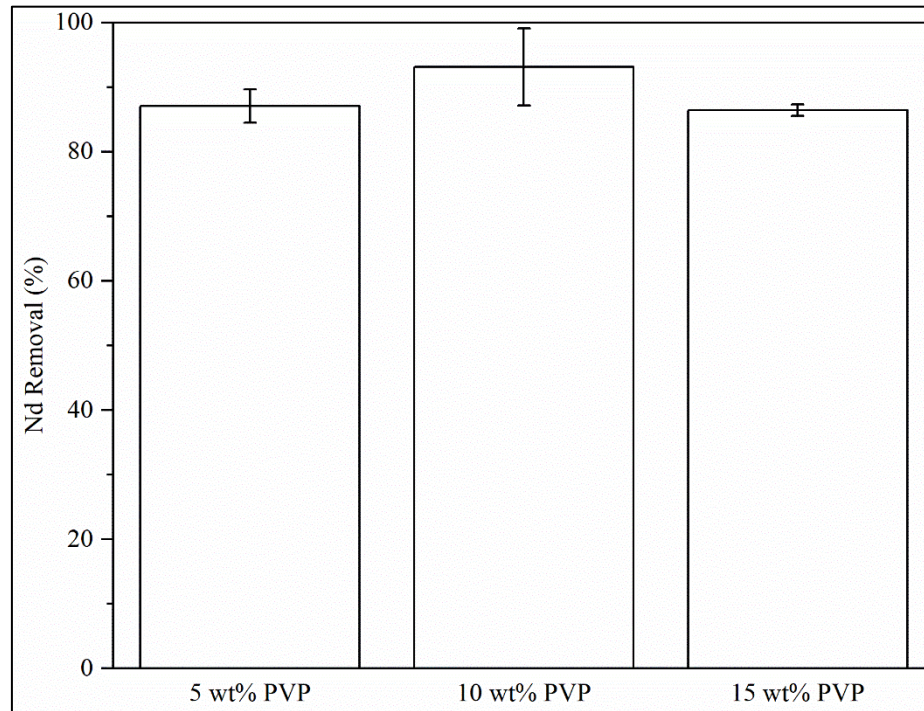
383    Yuan Xin Yeoh, Mazrul Nizam bin Abu Seman,
       Mohd Yusri bin Mohd Yunus and
       Abdul Wahab Mohammad

Effect of Polyvinylpyrrolidone Concentration in
the Substrate of Thin-Film Composite Forward
Osmosis Membrane on Neodymium Removal

**Figure 11.** Nd removal for TFC membranes prepared from different PVP concentrations in FO mode.

## CONCLUSION

The Nd removal using the TFC FO PES membrane with membrane substrate fabricated from different PVP concentrations was proven to be effective, where all the removal percentages were higher than 85%. Without PVP, the TFC membrane could not be used for the FO process. The FTIR spectra proved the presence of PVP in the substrate and PA in the active layer of TFC. Among all the PVP concentrations, the TFC membrane prepared from 10 wt% PVP was proven to be the most effective in Nd removal, achieving 93.11%, despite its high water flux and reverse salt flux. This can be attributed to the belt and extended leaf structure on the active layer. The membrane support prepared from 10 wt% PVP exhibited the highest porosity (88.88%), a moderate mean pore size (34.62 nm), the highest surface roughness (77.71 nm), a moderate specific reverse flux, the highest A value (0.6085 L/m$^2$·h·bar), the highest B value (1.4826 L/m$^2$·h), and a low S value (467.5225 μm). For future work, other parameters that affect the substrate morphology can be explored, such as the concentration of polymeric material and the gap size of the casting machine. Zeta potential characterisation should be conducted to determine the correlation between surface charge and REE removal. The application of TFC FO membrane in REE upstream and midstream recycling is a potential solution to the current issues faced by the REE industry.

## REFERENCES

1.  Paulick, H. and Machacek, E. (2017) The global rare earth element exploration boom: An analysis of resources outside of China and discussion of development perspectives. *Resources Policy*, **52**, 134–153.

2.  Wang, S., Xiong, Z., Wang, L., Yang, X., Yan, X., Li, Y., Zhang, C.and Liang, T. (2022) Potential hot spots contaminated with exogenous, rare earth elements originating from e-waste dismantling and recycling. *Environmental Pollution*, **309**, 119717.

3.  Gedam, V. V., Raut, R. D., Lopes de Sousa Jabbour, A. B. and Agrawal, N. (2021) Moving the circular economy forward in the mining industry: Challenges to closed-loop in an emerging economy. *Resources Policy*, **74**, 102279.

384   Yuan Xin Yeoh, Mazrul Nizam bin Abu Seman,
Mohd Yusri bin Mohd Yunus and
Abdul Wahab Mohammad

Effect of Polyvinylpyrrolidone Concentration in
the Substrate of Thin-Film Composite Forward
Osmosis Membrane on Neodymium Removal

4.   Goodman, A. J., Bednar, A. J.and Ranville, J. F. (2023) Rare earth element recovery in hard-rock acid mine drainage and mine waste: A case study in Idaho Springs, Colorado. *Applied Geochemistry*, **150**, 105584.

5.   Hermassi, M., Granados, M., Valderrama, C., Ayora, C. and Cortina, J. L. (2022) Recovery of rare earth elements from acidic mine waters: An unknown secondary resource. *Science of The Total Environment*, **810**, 152258.

6.   Shu, Q., Liao, C. -F., Zou, W. -Q., Xu, B. -Q. and Tan, Y. -H. (2021) Recovery of rare earth element ytterbium(III) by dried powdered biomass of spirulina: Adsorption isotherm, kinetic and thermo-dynamic study. *Transactions of Nonferrous Metals Society of China*, **31(4)**, 1127–1139.

7.   Li, C., Zhuang, Z., Huang, F., Wu, Z., Hong, Y. and Lin, Z. (2013) Recycling Rare Earth Elements from Industrial Wastewater with Flowerlike Nano-Mg(OH)2. *ACS Applied Materials & Interfaces*, **5(19)**, 9719–9725.

8.   Ren, M., Ning, P., Xu, J., Qu, G. and Xie, R. (2018) Concentration and treatment of ceric ammonium nitrate wastewater by integrated electrodialysis-vacuum membrane distillation process. *Chemical Engineering Journal*, **351**, 721–731.

9.   Pramanik, B. K., Shu, L., Jegatheesan, J., Shah, K., Haque, N. and Bhuiyan, M. A. (2019) Rejection of rare earth elements from a simulated acid mine drainage using forward osmosis: The role of membrane orientation, solution pH, and temperature variation. *Process Safety and Environmental Protection*, **126**, 53–59.

10.   Saleh, T. A. and Gupta, V. K. (2016) Chapter 1 - An Overview of Membrane Science and Technology. *Nanomaterial and Polymer Membranes. T. A. Saleh and V. K. Gupta, Elsevier*, 1–23.

11.   Halakarni, M. A., A. Samage, A. Mahto, V. Polisetti and S. K. Nataraj. (2023) Forward osmosis process for energy materials recovery from industrial wastewater with simultaneous recovery of reusable water: a sustainable approach. *Materials Today Sustainability*, **22**, 100361.

12.   Mohammadifakhr, M., de Grooth, J., Roesink,, H. D. W. and Kemperman, A. J. B. (2020) Forward Osmosis: A Critical Review. **8(4)**, 404.

13.   Carraretto, I. M., Ruzzi, V., Lodigiani, F., Colciaghi, R., Simonetti, R., Buzzaccaro, S., Molinaroli, L., Colombo, L. P. M., Piazza, R. and Manzolini, G. (2023) Characterization of the physical properties of the thermoresponsive block-copolymer PAGB2000 and numerical assessment of its potentialities in Forward Osmosis desalination. *Polymer Testing*, **128**, 108238.

14.   Sun, Z., Zhang S., Zhang Z., Yang Y., Zhang, C., Qian, Y. and Ren, X. (2023) A novel antifouling polyamide thin-film composite forward osmosis membrane fabricated by poly(m-phenylene isophthalamide) for seawater desalination. *Journal of Environmental Chemical Engineering*, **11(5)**, 110739.

15.   Blandin, G., Ferrari, F., Lesage, G., Le-Clech, P., Héran, M. and Martinez-Lladó, X. (2020) Forward Osmosis as Concentration Process: Review of Opportunities and Challenges. *Membranes (Basel)*, **10(10)**.

16.   Hou, D., Fan, H., Jiang, Q., Wang, J. and Zhang, X. (2014) Preparation and characterization of PVDF flat-sheet membranes for direct contact membrane distillation. *Separation and Purification Technology*, **135**, 211–222.

17.   Milescu, R. A., McElroy, C. R., Farmer, T. J., Williams, P. M., Walters, M. J. and Clark, J. H.. (2019) Fabrication of PES/PVP Water Filtration Membranes Using Cyrene®, a Safer Bio-Based Polar Aprotic Solvent. *Advances in Polymer Technology*, **2019**, 9692859.

18.   Ho, C. -C., Su, J. F. and Cheng, L. -P. (2021) Fabrication of high-flux asymmetric poly-ethersulfone (PES) ultrafiltration membranes by nonsolvent induced phase separation process: Effects of H2O contents in the dope. *Polymer*, **217**, 123451.

19.   Chun, Y., Mulcahy, D., Zou, L. and Kim, I. S. (2017) A Short Review of Membrane Fouling in Forward Osmosis Processes. *Membranes (Basel)*, **7(2)**.

20.   A. Aziz S. N. S., Abdul Rahman, A. F. H., Abu Seman, M. N. and Hilal, N. (2018) Comparison of the intrinsic parameters (A, B and S) of a forward osmosis membrane using pressurized and non-pressurized methods. *Desalination and Water Treatment*, **129**, 14–23.

21.   Singh, N., Petrinic, I., Hélix-Nielsen, C., Basu, S. and Balakrishnan, M. (2019) Influence of Forward Osmosis (FO) membrane properties on dewatering of molasses distillery wastewater. *Journal of Water Process Engineering*, **32**, 100921.

22.   Pavia, D. L., Lampman, G. M. and Kriz, G. S. (2001) Introduction to Spectroscopy, Tomson Learning Inc.

385    Yuan Xin Yeoh, Mazrul Nizam bin Abu Seman,
Mohd Yusri bin Mohd Yunus and
Abdul Wahab Mohammad

Effect of Polyvinylpyrrolidone Concentration in
the Substrate of Thin-Film Composite Forward
Osmosis Membrane on Neodymium Removal

23. Adnan, M., Zainuddin, M. I. F. and Ahmad, A. L. (2023) The Effect of Concentration on PES/NMP System on Flat Sheet Membrane Fabrication and its Performance for CO2 Gas Separation. *Journal of Physical Science*, **34**, 101–114.

24. Nasr, M., Alfryyan, N., Ali, S. S., Abd El-Salam, H. M. and Shaban, M. (2022) Preparation, characterization, and performance of PES/GO woven mixed matrix nanocomposite forward osmosis membrane for water desalination. *RSC Adv.*, **12(39)**, 25654–25668.

25. Moarefian, A., Golestani, H. A. and Bahmanpour, H. (2014) Removal of amoxicillin from wastewater by self-made Polyethersulfone membrane using nanofiltration. *Journal of Environmental Health Science and Engineering*, **12(1)**, 127.

26. Rafieian, F., Mousavi, M., Dufresne, A. and Yu, Q. (2020) Polyethersulfone membrane embedded with amine functionalized microcrystalline cellulose. *International Journal of Biological Macromolecules*, **164**, 4444–4454.

27. Hu, S., Liu, Y., Yin, Z., Chen, H., Jin, Y., Zhang, A., Zhang, M., Hua, L., Du, J. and Li, G. (2024) 3D printed polyvinylpyrrolidone–honey-gel with adhesive and degradable ability applied as bio-tape. *APL Materials*, **12(4)**.

28. Perera, D. H. N., Song Q., Qiblawey, H. and Sivaniah, E. (2015) Regulating the aqueous phase monomer balance for flux improvement in polyamide thin film composite membranes. *Journal of Membrane Science*, **487**, 74–82.

29. Lim, Y. J., Goh, K., Lai, G. S., Zhao, Y., Torres, J. and Wang, R. (2021) Unraveling the role of support membrane chemistry and pore properties on the formation of thin-film composite polyamide membranes. *Journal of Membrane Science*, **640**, 119805.

30. Gonzalez Ortiz, D., Nouxet, M., Maréchal, W., Lorain, O., Deratani, A. and Pochat-Bohatier, C. (2022) Immobilization of poly(vinyl pyrrolidone) in Polysulfone Membranes by Radically-Initiated Crosslinking Using Potassium Persulfate. *Membranes (Basel)*, **12(7)**.

31. Saljoughi, E. and Mohammadi, T. (2009) Cellulose acetate (CA)/polyvinylpyrrolidone (PVP) blend asymmetric membranes: Preparation, morphology and performance. *Desalination*, **249**(2), 850–854.

32. Ma, X. -H., Yao, Z. -K., Yang, Z., Guo, H., Xu, Z. -L., Tang, C. Y. and Elimelech, M. (2018) Nanofoaming of Polyamide Desalination Membranes To Tune Permeability and Selectivity. *Environmental Science & Technology Letters*, **5(2)**, 123–130.

33. Ye Jin, S., Jong Hoo, K., Ye Som, K., Sang Deuk, K., Young Hoon, C., Ho Sik, P., Seung Eun, N., You In, P., Eun Ho, S. and Jeong, F. K. (2018) Controlling the Morphology of Poly-vinylidene-co-hexafluoropropylene (PVDF-co-HFP) Membranes Via Phase Inversion Method. *Membrane Journal*, **28(3)**, 187–195.

34. Ismail, N., Jakariah, N., Bolong, N., Anissuzaman, S., Md. Nordin, N. A. H. and Razali, A.. (2017) Effect of Polymer Concentration on the Morphology and Mechanical Properties of Asymmetric Poly-sulfone (PSf) Membrane. *Journal of Applied Membrane Science & Technology*, **21**.

35. Ma, X., Yang, Z., Yao, Z., Guo, H., Xu, Z. and Tang, C. Y. (2019) Tuning roughness features of thin film composite polyamide membranes for simultaneously enhanced permeability, selectivity and anti-fouling performance. *Journal of Colloid and Interface Science*, **540**, 382–388.

36. Peng, L. E., Yao, Z., Yang, Z., Guo, H. and Tang, C. Y. (2020) Dissecting the Role of Substrate on the Morphology and Separation Properties of Thin Film Composite Polyamide Membranes: Seeing Is Believing. *Environmental Science & Technology*, **54(11)**, 6978–6986.

37. Qu, D. (2008) Wetting and Roughness. *Annual Review of Materials Research*.

38. Oymaci, P., Offeringa, P. E., Borneman, Z. and Nijmeijer. K. (2021) Effect of Osmotic Pressure on Whey Protein Concentration in Forward Osmosis. **11(8)**, 573.

39. Wang, Z., Zheng, J., Tang, J., Wang, X. and Wu, Z. (2016) A pilot-scale forward osmosis membrane system for concentrating low-strength municipal wastewater: Performance and implications. *Scientific Reports*, **6**, 21653.

40. Wolfe, T., Bourcier, W. and Metcalfe, P. (2011) Osmotic Pressure Calculation Using Pitzer Equation Modeling.

41. Ma, S., Wu, X., Fan, L., Wang, Q., Hu, Y. and Xie, Z. (2023) Effect of Different Draw Solutions on Concentration Polarization in a Forward Osmosis Process: Theoretical Modeling and Experimental Validation. *Industrial & Engineering Chemistry Research*, **62(8)**, 3672–3683.

42. Amrit, B., Simin, S. and Mohtada, S. (2017) Effect of Internal and External Concentration Polarizations on the Performance of Forward Osmosis Process. Osmotically Driven Membrane

386  Yuan Xin Yeoh, Mazrul Nizam bin Abu Seman,
Mohd Yusri bin Mohd Yunus and
Abdul Wahab Mohammad

Effect of Polyvinylpyrrolidone Concentration in
the Substrate of Thin-Film Composite Forward
Osmosis Membrane on Neodymium Removal

Processes. D. Hongbo, T. Audie and W. Xinying. Rijeka, IntechOpen: Ch. 4.

43. Kamel, A. H., Al-Juboori, R. A., al-shaeli, M., Ladewig, B., Ibrahim, S. S. and Alsalhy, Q. F. (2023) Potential application of hybrid forward osmosis – Membrane distillation (FO-MD) system for various water treatment processes. *Process Safety and Environmental Protection*, **180**, 1023–1052.

44. Zhao, P., Gao, B., Yue, Q., Kong, J., Shon, H. K., Liu, P. and Gao, Y. (2015) Explore the forward osmosis performance using hydrolyzed polyacrylamide as draw solute for dye wastewater reclamation in the long-term process. *Chemical Engineering Journal*, **273**.

45. Murat, E., Serkan, A., Derya, İ., Ebubekir, Y. and İsmail, K. (2018) Forward Osmosis Membranes – A Review: Part II. Osmotically Driven Membrane Processes. D. Hongbo, T. Audie and W. Xinying. Rijeka, IntechOpen: Ch. 3.

46. Lee, W., Kang, P., Kim, A. and Lee, S. (2018) Impact of surface porosity on water flux and structural parameter in forward osmosis. *Desalination*, **439**, 46–57.

47. Konsowa, A. H., AbdAllah, H. Z., Nosier, S. and Eloffy. M. G. (2022) Thin-film nanocomposite forward osmosis membrane for water desalination: synthesis, characterization and performance improvement. *Water Quality Research Journal*, **57(2)**, 72–90.

48. Kahrizi, M., Lin, J., Ji, G., Kong, L., Song, C., Dumée, L. F., Sahebi, S. and Zhao, S. (2020) Relating forward water and reverse salt fluxes to

membrane porosity and tortuosity in forward osmosis: CFD modelling. *Separation and Purification Technology*, **241**, 116727.

49. Liu, F., Wang, L., Li, D., Liu, Q. and Deng, B. (2019) A review: the effect of the microporous support during interfacial polymerization on the morphology and performances of a thin film composite membrane for liquid purification. *RSC Advances*, **9(61)**, 35417–35428.

50. Wang, Z., Zheng, J., Tang, J., Wang, X. and Wu, Z. (2016) A pilot-scale forward osmosis membrane system for concentrating low-strength municipal wastewater: performance and implications. *Scientific Reports*, **6(1)**, 21653.

51. Sark, J. F., Jullok, N. and Lau, W. J. (2021) Improving the Structural Parameter of the Membrane Sublayer for Enhanced Forward Osmosis. *Membranes (Basel)*, **11**(6).

52. Jang, H., Kang, S. and Kim, J. (2024) Identification of Membrane Fouling with Greywater Filtration by Porous Membranes: Combined Effect of Membrane Pore Size and Applied Pressure. **14(2)**, 46.

53. Hobbs, C., Hong, S. and Taylor, J. (2006) Effect of surface roughness on fouling of RO and NF membranes during filtration of a high organic surficial groundwater. *Journal of Water Supply Research and Technology-aqua*, **55**.

54. Xie, M., Price, W. E. and Nghiem, L. D. (2012) Rejection of pharmaceutically active compounds by forward osmosis: Role of solution pH and membrane orientation. *Separation and Purification Technology*, **93**, 107–114.